On Intrinsic Alignment: Large Scale, Linear, But not Gaussian

Lam Hui

Jun Zhang

Why intrinsic alignment?

- Study angular momentum build-up of galaxies
- Interpretation of weak lensing

1984ApJ...286...38W

which grows at first order. We may thus write (3) to sufficient accuracy as

$$J(t) = \rho_0 a^5 \int_{S_L} (\boldsymbol{q} - \bar{\boldsymbol{q}}) \times \dot{\boldsymbol{x}} d^3q + \rho_0 a^5 \int_{\Sigma_{S_L}} (\boldsymbol{q} - \bar{\boldsymbol{q}}) \times \dot{\boldsymbol{x}} b \nabla\varphi \cdot d\boldsymbol{S} ,$$

where to first order

$$\bar{\boldsymbol{q}}(t) = \frac{1}{V_L} \int_{\Sigma_{S_L}} \boldsymbol{q} b \nabla\varphi \cdot d\boldsymbol{S} .$$

Making this substitution, using our result (11) and retaining only second-order terms,

$$J(t) = -\rho_0 a^5 b\dot{b} \int_{\Sigma_{S_L}} \boldsymbol{q} \times (\nabla\varphi - \overline{\nabla\varphi}) \nabla\varphi \cdot d\boldsymbol{S} . \tag{12}$$

This result can be written more suggestively as

$$J(t) = -\frac{b}{\dot{b}} \int_{\Sigma_{S_E}} \boldsymbol{r} \times (\boldsymbol{v} - \bar{\boldsymbol{v}}) \rho \boldsymbol{v} \cdot d\boldsymbol{S} , \tag{13}$$

where the integral is now taken over the surface of the Eulerian sphere. This shows that the Eulerian sphere gains angular momentum purely as a result of convective transport across its boundary and not as a result of torques acting on the matter interior to it. The connection with Peebles's analysis can be made by converting equation (12) into a volume integral

$$J(t) = -\rho_0 a^5 b\dot{b} \int_{S_L} \{(\nabla^2\varphi)\boldsymbol{q} \times (\nabla\varphi - \overline{\nabla\varphi}) + \boldsymbol{q} \times [(\nabla\varphi \cdot \nabla)\nabla\varphi]\} d^3q .$$

The second term in the integrand can be converted back to a surface integral which vanishes on Σ_{S_L}. This leaves

$$J(t) = -\rho_0 a^5 b\dot{b} \int_{S_L} \nabla^2\varphi \boldsymbol{q} \times (\nabla\varphi - \overline{\nabla\varphi}) d^3q . \tag{14}$$

Using $\delta(\boldsymbol{q}) = b\nabla^2\varphi$ and converting from Lagrangian back to Eulerian variables, this is equal at second order to

$$J(t) = \rho_0 a^2 \int_{S_E} \delta(\boldsymbol{x}) \boldsymbol{x} \times (\dot{\boldsymbol{x}} - \bar{\dot{\boldsymbol{x}}}) d^3x , \tag{15}$$

which is the Eulerian expression which Peebles used to calculate $\boldsymbol{J}$.

IV. EXPERIMENTAL VERIFICATION

I have attempted to verify the results of § II in two 32,768 particle N-body experiments which are part of an ongoing collaborative program to study clustering in an expanding universe (Frenk, White, and Davis 1983; White, Frenk, and Davis 1983; Efstathiou *et al.* 1984). Both simulations used a particle-mesh method on a 64^3 grid to calculate forces and advance the particles. One experiment was designed to study a neutrino-dominated universe (White, Frenk, and Davis 1983). Its density field began with an rms δ of 22% and a large coherence length. It was allowed to expand by a factor of 20. The other experiment began with a Poisson distribution of particles within the computational volume and was allowed to expand by a factor of 32. The evolution of these models can be taken to represent the formation of structure in the "pancake" and hierarchical clustering pictures, respectively. In both, the background universe was taken to be flat and initial velocities were set so that only the growing mode was present. In the last time frame of each experiment I identified clusters by linking particles with separations smaller than 0.4 of the mean interparticle spacing, and then joining all "friends of friends." This procedure resulted in clusters with mean δ values in the range 50–400. Finally I calculated the angular momentum at earlier times of those particles which ended up in each of these clusters.

Figure 1 illustrates the growth of angular momentum in these models. For the members of each cluster, I took $J(t)$ and divided it by $a^{3/2}J(t_i)$, where t_i is the initial time. If growth obeys the theory of § II this quantity should remain equal to unity. For each simulation the figure shows the average of its logarithm as a function of time for clusters with more than 100 members. (The largest clusters in each simulation had $2\text{–}3 \times 10^3$ members.) In addition, the evolution of four "typical" clusters is shown for each simulation. The theoretical prediction is followed closely at small expansion factors. However, as a increases, the density contrast of clusters becomes large and angular momentum transfer to them ceases

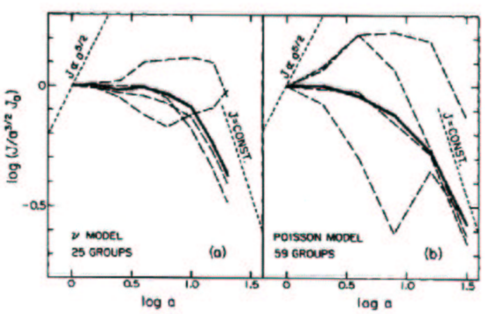

white 84

FIG. 1.—Angular momentum normalized to the value predicted by linear theory is shown as a function of expansion factor for the particles which end up in groups of more than 100 members in two N-body experiments. Fig. 1*a* is a simulation of a neutrino-dominated universe, while in Fig. 1*b* the particles were initially distributed uniformly at random. Solid lines show the mean for all rich groups in each model while dashed lines show the behavior of "typical" individual groups. The dotted lines show the relationships $J \propto a^{5/2}$ which would be obeyed if angular momentum grew at second order in perturbation theory, and J = const which is expected at late times.

How does intrinsic alignment arise?

- Tidal torque-up of halos

(Doroshkevich 70, Peebles 69, White 84)

$$\vec{L} = \int d^3q\, \rho\, \vec{r} \times \vec{v}$$

$$L_i \sim \epsilon_{ijk} I_{kl} \underline{\nabla_j \nabla_l \phi}$$

- Long range correlation in ϕ leads to correlation in L

(Lee & Pen, Croft & Metzler, Catelan et al. Heavens et al. Crittenden et al. Mackey et al...)

- Nonlinear effects

(Porciani et al. Vivitska et al von den Bosch et al.)

What determines ellipticity ϵ ?

- 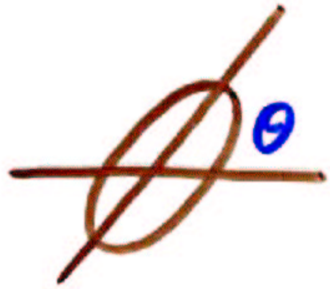

  $\epsilon_1 = |\epsilon| \cos 2\theta$

  $\epsilon_2 = |\epsilon| \sin 2\theta$

- $\epsilon_1 \sim (L_x^2 - L_y^2) f$

  $\epsilon_2 \sim 2 L_x L_y f$

- $\epsilon \sim L^2 \sim \nabla\phi \cdot \nabla\phi$

Brown et al.

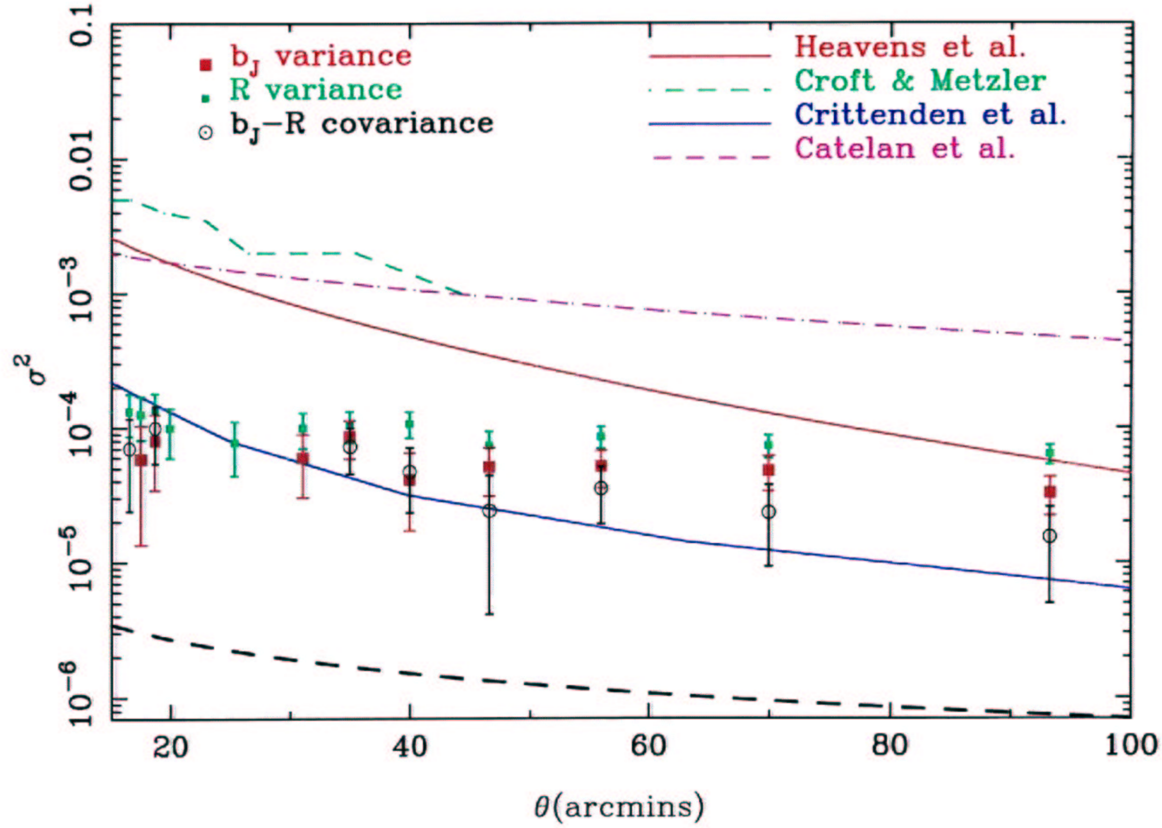

Usual Argument:

Assume ϕ Gaussian

$$\langle \epsilon(1)\, \epsilon(2) \rangle \sim \langle \phi(1)\phi(1)\phi(2)\phi(2) \rangle$$

$$\sim \langle \phi(1)\, \phi(2) \rangle^2$$

(note: $\langle \epsilon(1) \rangle = \langle \epsilon(2) \rangle = 0$)

$$\langle \epsilon(1)\epsilon(2) \rangle \sim \xi_{12}^2$$

Gravity makes ϕ non-Gaussian even if it starts off Gaussian.

non-Gauss. part

$$\langle \epsilon(1)\, \epsilon(2) \rangle \sim \langle \phi(1)\phi(1)\phi(2)\phi(2) \rangle_c$$

$$\sim \underline{\langle \phi(1)\phi(2) \rangle} \langle \phi(1)^2 \rangle \langle \phi(2)^2 \rangle$$

$$+ \ldots$$

1 point

$$\langle \epsilon(1)\, \epsilon(2) \rangle \propto \xi_{12} \text{ on large scales!}$$

Baugh, Gaztanaga, Efstathiou 95

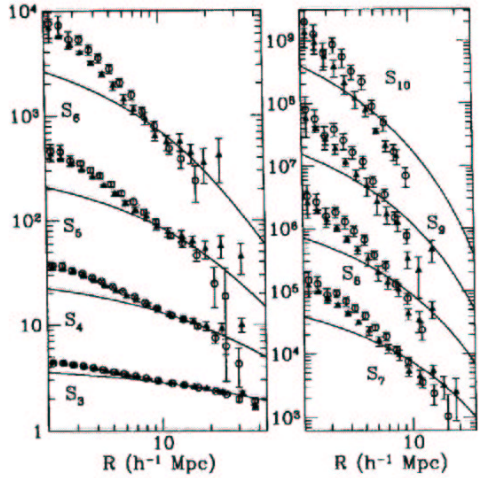

Figure 13. The hierarchical amplitudes $S_J = \bar{\xi}_J/\bar{\xi}_2^{J-1}$ for $\sigma_8 = 1.0$ averaged over 10 simulations with $L_B = 300\,h^{-1}$ Mpc, $N = 100^3$ (circles) and over five simulations with $L_B = 378\,h^{-1}$ Mpc, $N = 126^3$ (triangles).

$$\frac{\xi_N}{\xi_2^{N-1}}$$

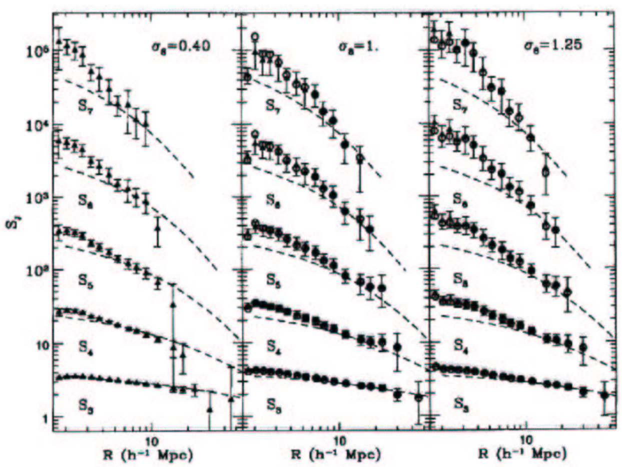

Figure 14. The hierarchical amplitudes $S_J = \bar{\xi}_J/\bar{\xi}_2^{J-1}$ in the $L_B = 180\,h^{-1}$ Mpc, $N = 64^3$ simulations for different output times: $\sigma_8 = 0.40, 1.0, 1.25$. The dashed line shows the PT approximation. Triangles correspond to the values averaged over 10 different realizations of the initial displacements from a grid (the error bars are the dispersion around the mean). Circles correspond to the average over 10 different realizations of the displacements from a glass.

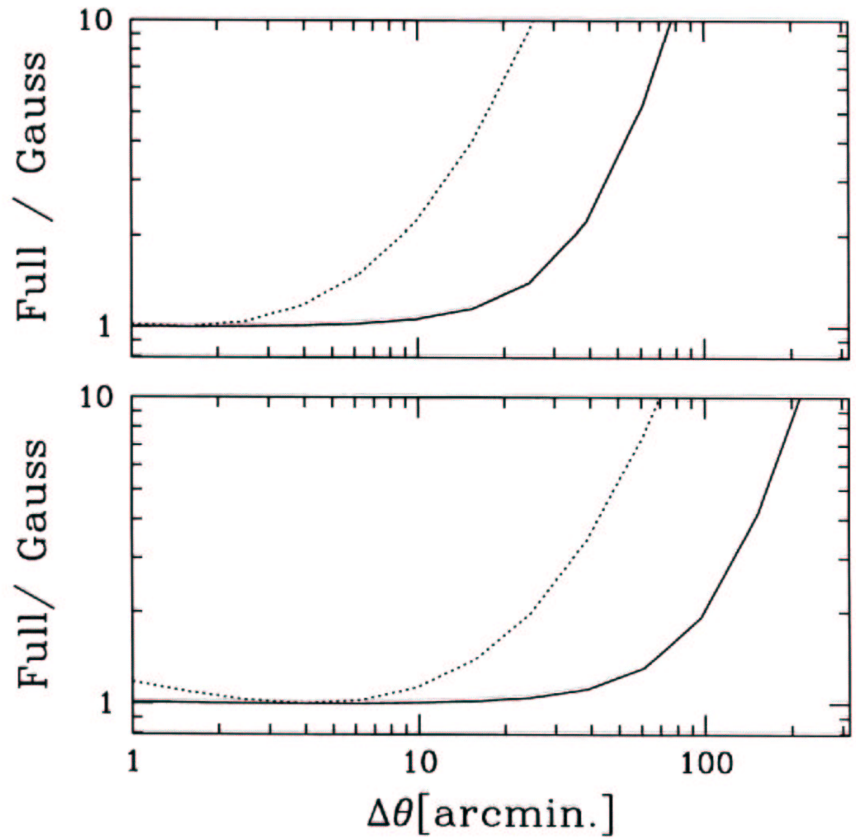

— $z_T = 50$

LH, Zhang 02

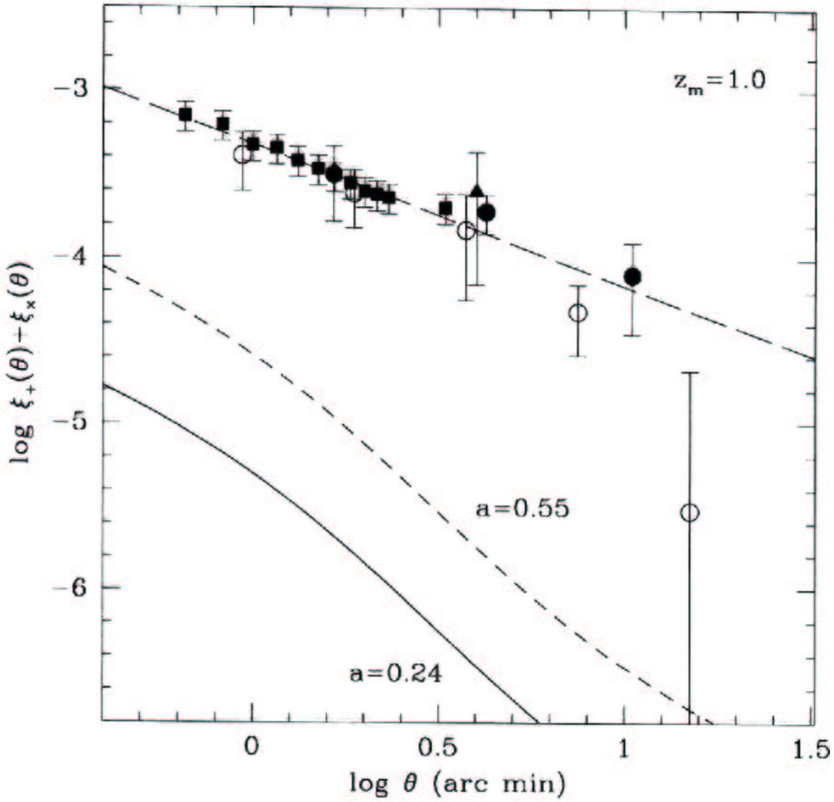

Crittenden et al.

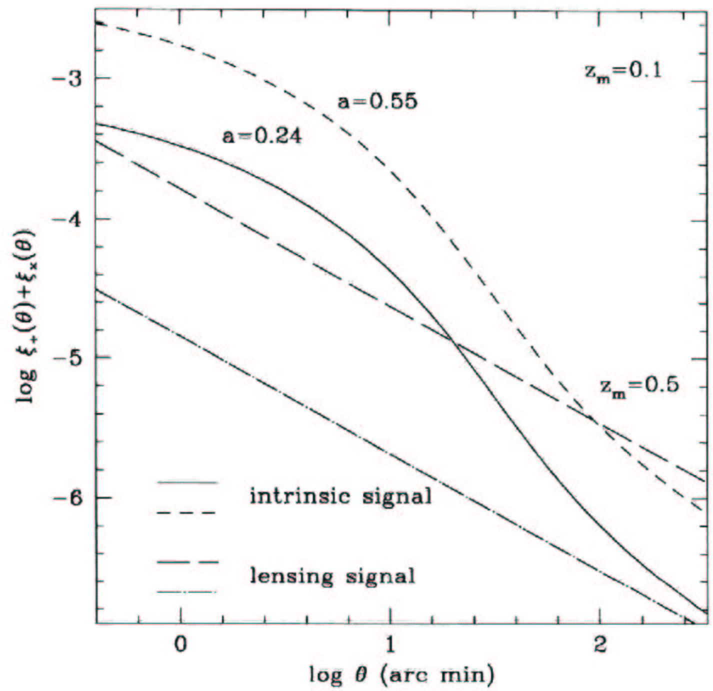

Crittenden et al.

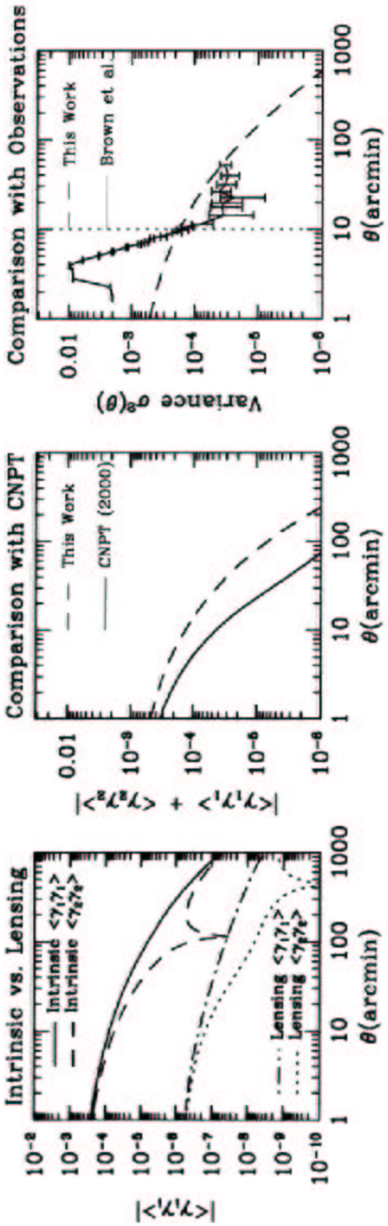

Mackey et al.

Intrinsic density-ellipticity correlation $\delta - \epsilon$

$$\langle \delta(1)\, \epsilon(2) \rangle \sim \langle \phi(1)\, \phi(2)\, \phi(2) \rangle \propto \xi_{12}$$

Galaxy-galaxy lensing measures the same

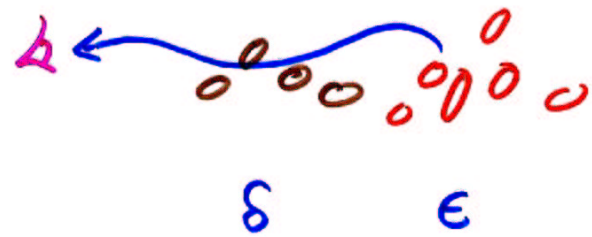

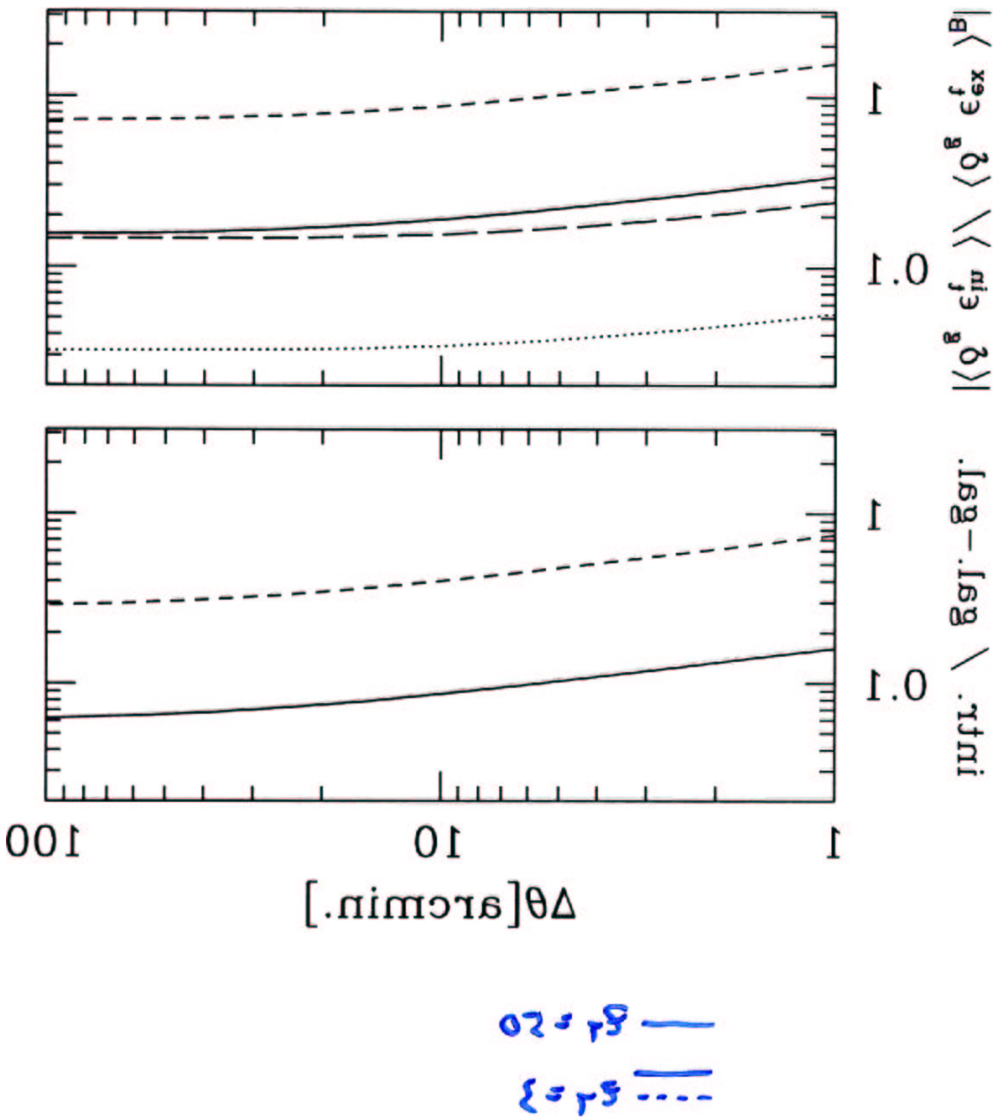
Δθ[arcmin.]
100
10
1
0.1
1

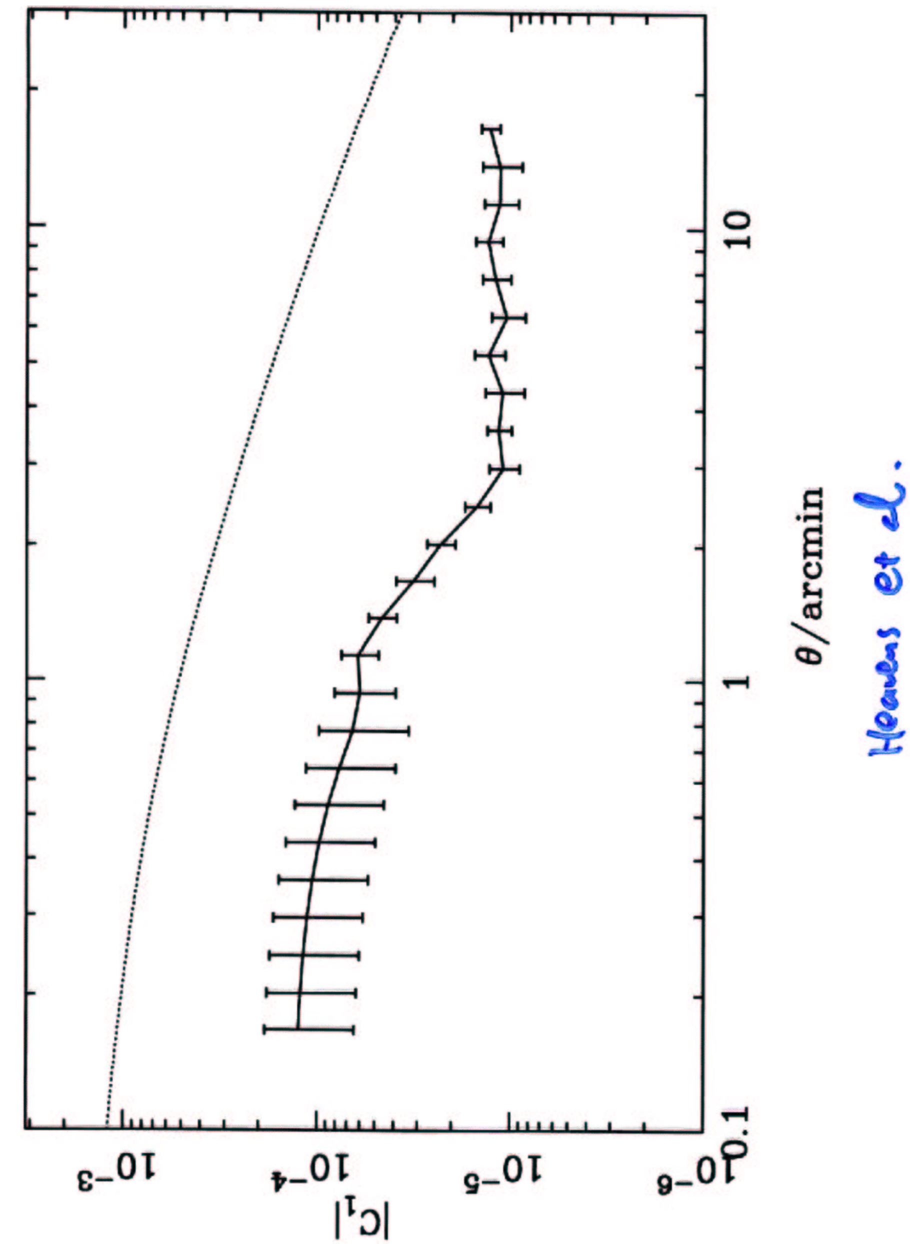
θ/arcmin
|C1|
10^-3
10^-4
10^-5
10^-6
0.1
1
10
Heavens et al.